



LUND UNIVERSITY

Continuous electrical imaging for mapping aquifer recharge along reaches of the Namoi River in Australia

Kelly, B.F.J.; Allen, D.; Ye, K.; Dahlin, Torleif

Published in:
Near Surface Geophysics

DOI:
[10.3997/1873-0604.2009024](https://doi.org/10.3997/1873-0604.2009024)

2009

[Link to publication](#)

Citation for published version (APA):

Kelly, B. F. J., Allen, D., Ye, K., & Dahlin, T. (2009). Continuous electrical imaging for mapping aquifer recharge along reaches of the Namoi River in Australia. *Near Surface Geophysics*, 7(4), 259-270.
<https://doi.org/10.3997/1873-0604.2009024>

Total number of authors:
4

General rights

Unless other specific re-use rights are stated the following general rights apply:
Copyright and moral rights for the publications made accessible in the public portal are retained by the authors and/or other copyright owners and it is a condition of accessing publications that users recognise and abide by the legal requirements associated with these rights.

- Users may download and print one copy of any publication from the public portal for the purpose of private study or research.
- You may not further distribute the material or use it for any profit-making activity or commercial gain
- You may freely distribute the URL identifying the publication in the public portal

Read more about Creative commons licenses: <https://creativecommons.org/licenses/>

Take down policy

If you believe that this document breaches copyright please contact us providing details, and we will remove access to the work immediately and investigate your claim.

LUND UNIVERSITY

PO Box 117
221 00 Lund
+46 46-222 00 00

Continuous electrical imaging for mapping aquifer recharge along reaches of the Namoi River in Australia

B.F.J. Kelly^{1,5*}, D. Allen^{2,5}, K. Ye^{3‡} and T. Dahlin⁴

¹ Connected Waters Initiative, University of New South Wales, School of Biological Earth and Environmental Science, 2052 Sydney, New South Wales, Australia

² Groundwater Imaging Pty Ltd, 279 Fitzroy Street, 2830 Dubbo, New South Wales, Australia

³ URS Australia Pty Ltd, Level 3, 116 Miller Street, 2060 North Sydney, New South Wales, Australia

⁴ Department of Engineering Geology, Lund University of Technology, PO Box 118, 221 00 Lund, Sweden

Received January 2008, revision accepted May 2009

ABSTRACT

In this study the capacity of towed floating electrical imaging for mapping a known aquifer recharge zone in more detail is investigated. A 50 km reach of the Namoi River, Australia, was surveyed. The river is perched up to 16 m above an unconfined aquifer that extends to 30 m below the ground surface. The unconfined aquifer overlies a semi-confined aquifer system. The electrical array consists of two current electrodes near the boat, followed by nine potential electrodes. The sequence of 1D electrical sounding curves generated was automatically inverted to obtain a layered earth electrical model along the river to a depth of approximately 40 m. There was weak correlation between the water conductivity measured in boreholes and the layered earth electrical model. Lithological logs from boreholes near the river indicate that the major layers seen in the electrical conductivity cross-section correspond to the major sedimentary units. Groundwater mounding in the vicinity of the river has been monitored after flooding. The groundwater flood mounds coincide with the location of the predominantly low electrically conductive sediments mapped beneath the river. This suggests that aquifer recharging waters migrate via the sands and gravels, then pool at the water table before dissipating. This survey demonstrates that mapping intervals of low electrically conductive sediments beneath the river maps potential aquifer recharge pathways.

INTRODUCTION

This case study presents a continuous electrical imaging survey, which generates a sequence of 1D electrical sounding curves along a known recharge interval on the Namoi River, Australia (Fig. 1). Due to irrigation abstractions the river is perched above the underlying unconfined alluvial aquifer. It is connected at Mollee Weir and disconnected by 16 m at Gunidgera Weir, based on borehole water head measurements since 1972 (NSWG 2007). This electrical imaging survey is part of a wider investigation of aquifer management in the Namoi Catchment. This study explores the value of electrical imaging for providing information between the river flow gauging stations and nearby boreholes on the electrical properties of the sediments that relate predominantly to the sediment type, pore water content, pore water salinity and degree of saturation. Sediments along the river and in the underlying aquifers range from gravels and sand to intervals of highly electrically conductive clay (smectite). Water in the river at the time of

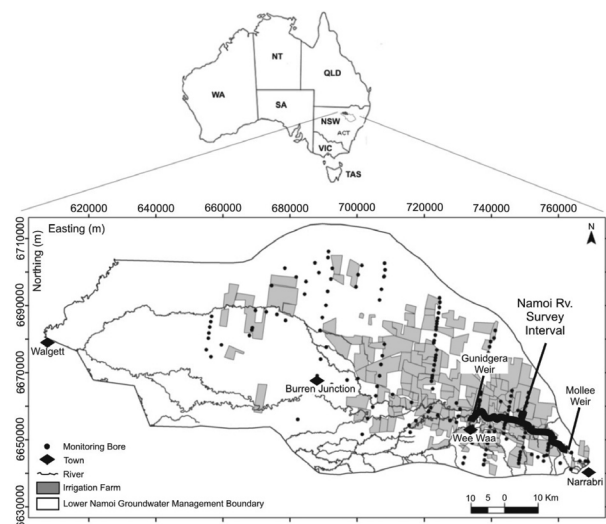


FIGURE 1
Location of the Namoi River, New South Wales, Australia. The surveyed reach was between Mollee and Gunidgera weirs (MGA94 grid coordinates, Universal Transverse Mercator projection).

* bryce.kelly@unsw.edu.au

‡ Previously at the National Centre for Groundwater Management, University of Technology, Sydney, Australia

the survey was approximately $500 \mu\text{S}/\text{cm}$. Anomalies indicated by the electrical imaging delineate reaches of the river for subsequent detailed investigations to quantify the reason for the anomalies and to determine how this is related to the hydraulic connection between the aquifer and river.

There have been numerous investigations in the past of the link between the river and the aquifer (Merrick 2000; Young *et al.* 2002; Triantafylis *et al.* 2003; McLean 2003). Previous studies were undertaken on a spacing that was too coarse (kilometres to tens of kilometres) to be able to accurately delineate, on the order of tens of metres, reaches of the Namoi River where recharge to the aquifer is occurring. To obtain higher resolution information to focus future river/aquifer studies a geophysical survey was undertaken.

A towed floating electrical imaging array has significant advantages compared to land based imaging methods. Surveying 20 km per day is easily achievable along a river, even when there are numerous fallen trees to be negotiated. Land based resistivity imaging using similar electrode spacing would only achieve about 1 km per day. Towed transient electromagnetic surveying techniques (Barrett *et al.* 2002; Barrett *et al.* 2006; Hatch *et al.* 2007; Tan *et al.* 2007) can have similar speed of coverage but lack the same near-surface vertical resolution. Given the advantages of the floating electrical imaging system it was selected for the geophysical survey with the aim of delineating in more detail the sedimentary units of the aquifer in order to map pathways of

high hydraulic conductivity between the river and the aquifer.

Groundwater in the alluvial sequences underlying the Namoi River is an important resource for the agriculture sector. The rapid expansion of the irrigation industry in the region since the early 1960s has led, in some areas, to the mining of the aquifer and in places the river has become disconnected from the underlying aquifer (Williams *et al.* 1989; Merrick 2000). There has been a cultural shift (away from mining the aquifer) in how groundwater is to be used in the region and current management goals aim to balance environmental considerations with a viable agricultural sector.

If the environmental impacts of groundwater extractions are to be better understood and groundwater within the region is to be used in a sustainable manner then it is important to understand the pathways of water movement both above and below ground. An important aspect of studying the pathways of connection is delineating where the aquifer is recharged. Knowing where the recharge areas are allows for these zones to be protected from development and also allows enhanced aquifer recharge to be explored.

River hydrographs located at Mollee Weir (near Narrabri) and Gunidgera (near Wee Waa) indicate that along this reach the Namoi River is constantly losing water to the aquifer. These two streamflow gauging locations are approximately 50 km apart. This interval is also an important recharge zone during floods (Merrick 2000).

The site is situated on open plains of unconsolidated sediment approximately 100 m thick. The land slopes gently from 205 m.a.s.l at Narrabri to 190 m.a.s.l near Wee Waa. Basement depth is less in the east and the river flows west. Figure 2 shows how the river is incised about 8 m into the surrounding floodplain. Palaeochannels bifurcate from the upstream extent of the present river course and splay out across the floodplain principally in a north-westerly direction. Palaeochannels at depth are evident from borehole data indicated by variations in basement depth, coarse sediment concentrations and groundwater chemistry (McLean 2003). Shallow palaeochannel locations are evident from soil and vegetation observation and a significant shallow palaeochannel bifurcates, to the north-west, from the current river course about half way along the surveyed length (Young *et al.* 2002). Differences in meander characteristics indicate that palaeochannels in the survey area were formed by higher flow regimes than the present day channel (Young *et al.* 2002). The soils of the region consist of clayey alluvium, which range from 6–15 m in thickness (Ward *et al.* 1999; Ward 1999). This is underlain by sequences of sand, gravel and clay.

Sediments in the region fill a valley carved out during pre-Tertiary times into Jurassic and Cretaceous sedimentary rocks. The sediments have been divided into three broad categories based on palynology investigations by Martin (1979, 1981, 1991). McLean (2003) summarizes the unconsolidated sediment geology. The uppermost formation is the Narrabri Formation, which predominantly consists of clays with minor sand and



FIGURE 2

The towed floating electrical imaging array passing irrigation pumps on the lower Namoi River. Electrodes, defined by the blue flotation tubing in the photograph, extend for 156 m behind the boat and around the bend in the river.

gravel beds. This unit is approximately 30 m thick and the sediments date from the Pleistocene to Recent. It is this formation that contains the unconfined aquifer that is the subject of the electrical imaging study. Underlying the Narrabri Formation is the Gunnedah Formation, which consists predominantly of gravel and sand with minor clay beds. These sediments date from the Pliocene to early Pleistocene. This is the productive aquifer used for irrigation. At the base of the alluvial sequence in the northern portion of the lower Namoi is the Cubbaroo Formation, middle to late Miocene and it consists of sand and gravel with interbedded brown to yellow and grey clay. Cubbaroo Formation sediments infill the pre-Tertiary channel. The Gunnedah Formation aquifer is semi confined from the overlying unconfined aquifer of the Narrabri Formation.

Continuous electrical imaging on water has been successfully undertaken both worldwide (Cherkauer *et al.* 1987; Cherkauer and Taylor 1990; Snyder *et al.* 2002; Loke and Lane 2004; Ball *et al.* 2006; Day-Lewis *et al.* 2006; Mansoor and Slater 2007; Nyquist *et al.* 2008) and in Australia (Barrett *et al.* 2002, 2006; Allen and Merrick 2007; Hatch *et al.* 2007; Tan *et al.* 2007). These previous investigations have been used to map changes in water quality, to delineate zones of water movements between the stream and underlying aquifer and to define variations in sediment type. Prior to the survey being undertaken it was uncertain if the electrical imaging would provide significant beneficial information on the lithology of the recharge zone because of two challenges. The region has zones of highly conductive clay and groundwater salinity is variable throughout the region, making it difficult to determine if electrical conductivity changes are due to

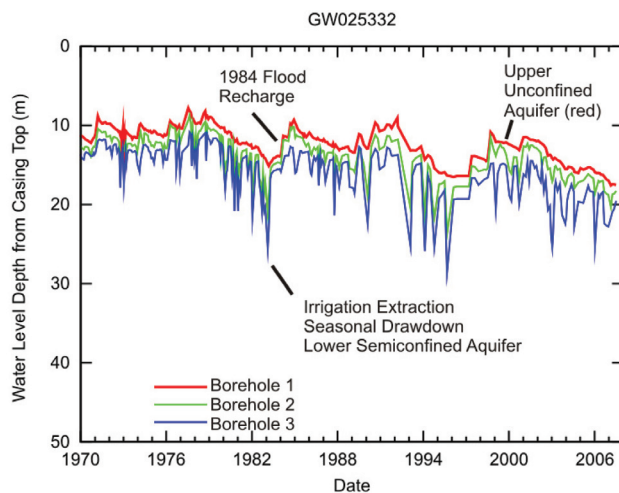


FIGURE 3 Groundwater monitoring borehole hydrographs. Borehole 1 is in the unconfined aquifer and is slotted from 17.7–21.4 m. The large rises in head observable in borehole 1 are due to recharge from flood water. Boreholes 2 and 3 are in the semi-confined aquifer. Borehole 2 is slotted from 38.1–41.1 m and borehole 3 is slotted from 50.9–55.5 m. Water used for irrigation is extracted from the semi-confined aquifer.

the clay context or pore water salinity. To constrain the interpretation the electrical imaging was compared to the lithological descriptions and water salinity measurements at a limited number of groundwater monitoring boreholes.

This project had three aims. Firstly, to see if the electrical imaging could delineate the major sedimentary features observed in boreholes adjacent to the river where the lithology was known. Secondly, to extend the interpretation to sections between the boreholes in order to map the sand and gravel recharge beds and to determine if there is a preferential pathway of connection between the river and the underlying aquifer. Thirdly, to interpret the resistivity image in the context of the groundwater recharge mound that occurred as a result of flooding in the region in 1984. Each time flood waters migrate along the river the water level in the unconfined aquifer rises from the recharge. At location GW025332 there are three boreholes (Fig. 3). Borehole 1 is slotted from 17.7–21.4 m below the ground surface. This borehole is located 200 m south of the river, where the ground surface was approximately 10 m above the river water level at the time of the survey. The recorded water level at the time of the survey was 17 m below the ground surface. The rise in head due to the 1984 flood is clearly observable at this location. The head rise due to flood waters for all bores near the river is analyzed further in the section on regional borehole data.

The Namoi River is a regulated river system with peak flows in summer and minimal flows in winter. The peak summer flows are due to dam releases for irrigating cotton. The water is stored in dams at the head of the Namoi River and is delivered to the irrigation farms via the Namoi River. The electrical imaging was undertaken in January 2006 during the peak of the irrigation season on a flow of about 800 megalitres per day.

PREVIOUS INVESTIGATIONS

Past groundwater hydrograph analysis, borehole water chemistry and regional EM38 investigation have all indicated that recharge to the aquifer occurs in the river interval of interest between Narrabri and Wee Waa. State government agencies have installed 588 groundwater monitoring boreholes throughout the lower Namoi catchment at 272 sites (NSWG 2007). The majority of these boreholes were installed in the 1950s, 1960s and 1970s to define the groundwater resource and monitor the expansion of the irrigation industry. At each borehole location there are two to seven piezometres monitoring different intervals of the aquifer. Water levels have been recorded in these boreholes four times per year for approximately 50 years.

Major ion and isotope investigations of the groundwater in the lower Namoi area have been undertaken by Calf (1978) and McLean (2003). Recharge along the reach of the Namoi River between Narrabri and Wee Waa is indicated by carbon (Calf 1978; McLean 2003) and tritium isotope analyses (McLean 2003).

Streamflow gauging at Mollee Weir and Gunidgera Weir indicates that the interval surveyed is a losing reach. Borehole

hydrographs spaced one or more kilometres apart along the river (Fig. 1) also indicate that the river recharges the aquifer in the surveyed interval. To replicate the stream and borehole hydrographs as part of a regional MODFLOW model Merrick (2000) incorporated river leakage to the aquifer in the Narrabri to Wee Waa interval. The 1984 flood, analysed further below, contributed about 80 GL of recharge to the aquifer system and continuous river recharge contributes on average 41 GL/year.

Triantafyllis *et al.* (2003) calibrated EM34 electromagnetic induction measurements (horizontal coils at 10 m, 20 m and 40 m spacing at 6300 Hz, 1600 Hz and 400 Hz, respectively) against previous soil and borehole hydrogeological investigations and delineated prior stream channels beyond the extent of the present Namoi River. This survey was undertaken on a 1 km grid spacing, so while it was able to map potential regional scale recharge zones, it did not have the resolution required for investigating the connection of the river with the underlying aquifer.

Rahman (2005) undertook a statistical cluster analysis (Davis 2002) of 47 borehole hydrograph sets and showed that boreholes near the river clustered into a distinct group compared to other hydrographs throughout the lower Namoi catchment. This group of bores had a clear response to high flows moving along the Namoi River.

TOWED FLOATING ELECTRICAL IMAGING EQUIPMENT

Electrical conductivity (EC) imaging in a vertical cross-section beneath the river was achieved using a towed floating electrical imaging array and a global positioning system (GPS). The principles of operation for the electrical array are presented in Fig. 4. Combinations of two current transmitting and two voltage receiving electrodes are used to sample volumes of ground proportional to the separation of those electrodes. The depth of investigation is increased by increasing the spacing between the potential electrodes and by moving the current and potential dipoles further apart.

A 156 m long floating electrode array was towed with a small boat (Fig. 2). The geometry of the positioning of the transmitting (T_x) and receiving electrodes (R_x) is shown in Fig. 4. Two transmitter electrodes separated by 16 m, positioned near the boat, are followed by receiver electrodes spaced at the following distances (in metres) from the end of the second transmitter electrode – 0.5, 1, 2, 4, 8, 16, 32, 64 and 128. Adjacent pairs of potential electrodes are sampled at each location to generate the 1D sounding curve at that point. Spacing the potential electrodes on a geometric sequence starting at 0.5 m with a common ratio of 2 results in 1D effective depths of investigation on a logarithmic scale at approximately one third of the potential electrode spacing (Allen and Merrick 2007). The 1D effective depth is defined as the depth from which 50% of the signal received by an array comes from both above and below that depth, assuming that the array is situated on the surface of a homogeneous half-space (Edwards 1977). For the array used the deepest effective depth of investigation is approxi-

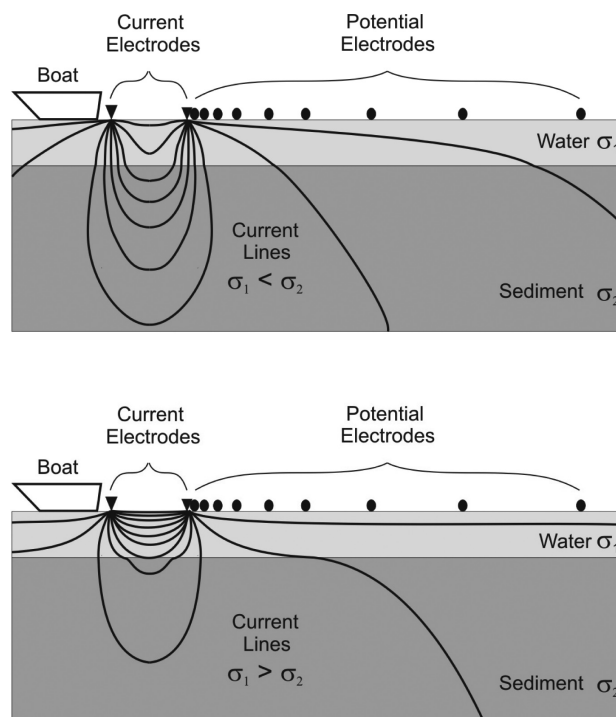


FIGURE 4

Principles of operation of the floating electrical imaging array. Current is injected using two electrodes. Electric fields emanate from the electrodes and are distorted as they cross electrical conductivity contrast boundaries ($\sigma =$ conductivity of the water and sediment layers). A series of exponentially spaced potential electrodes detect the distortion of the field. The field distribution depends on the relative electrical conductivities of the layers.

mately 22 m. The array was designed around the 1D effective depth theories. Both 1D and 2D sensitivity are discussed further in the separate section on sensitivity below.

The array used 0.5 m long transmitting electrodes that facilitate better signal-to-noise ratios through increased current injection. Software (HydroGeoImager (Allen 2007b)) was especially designed for processing data from such arrays.

The floating array was designed so that it would slide past obstacles easily and have minimum drag that causes problems with cross track drift when cornering. Flotation was provided by Layflat tubing, which could be deflated in order to pack the array for transportation. Further details of the array design are given in Allen (2007).

The geo-electric transceiver utilized was a combination of a Terraohm RIP924b with an ABEM SAS2000. The system continuously transmitted a bipolar waveform with a current of at least 100 mA, however, currents of 200 mA and 500 mA were transmitted at times. The transceiver measured the signal coming from the eight quadrupoles simultaneously and the data were stacked into stored records approximately every ten seconds. Gain/attenuation of each channel was sufficient to keep the signal-to-instrument-noise ratio (SNR) to at least above three for 99% of the river length surveyed.

Canal depth is required for interpretation of the EC imaging and therefore was measured. River depth was recorded using a Garmin GPSMap188 sonar device with a blanking distance of around 1.1 m. Sonar sampling occurred at least once every two seconds. The water depth varied from 0.2–5 m along the centre line of the river.

The boat position was logged at regular intervals of time and/or distance using a GPS. During times of poor GPS signal reception, the operator paused surveying. There were also sections of the river where fallen trees and rapids prevented surveying; these intervals have been left blank in the figures below. The survey speed was kept below 9 km/hr to reduce noise in the received signal. What caused the noise is not known but it is most likely due to streaming potentials at the electrodes. The signal noise was removed by surveying at a low speed where this noise was absent. Placing the potential electrodes in their correct X and Y position was achieved using a combination of the boat speed and the tracked GPS position. This was particularly important for the potential electrode at 128 m. As shown in the sensitivity discussion below, the survey is not sensitive to the last electrode, thus the small error in the placement of the last electrode did not significantly influence the measured electrical properties.

Electrical imaging or galvanic surveys have traditionally been presented in units of resistivity but because most water managers talk in units of electrical conductivity, particularly micro-siemens per centimetre, this paper is presented in these units.

Array sensitivity

Determining the depth of investigation of an array requires that assumptions be made about the vertical and lateral continuity of electrical layers within the Earth. The derivation of the sensitivity equations is discussed in Loke (2004), Roy and Apparao (1971) and McGillivray and Oldenburg (1990). In horizontally layered environments, typical of palaeovalleys infilled with alluvial sediments, if it is assumed that the layers extend continuously laterally (the *x*- and *y*-dimensions of the layer extending from $-\infty$ to ∞), then for the general four electrode array the 1D sensitivity, in the form of the vertical response function (Merrick 1997) is calculated from

$$W(z) = 4z \frac{[(r_{11}^2 + 4z^2)^{-3/2} - (r_{12}^2 + 4z^2)^{-3/2} - (r_{21}^2 + 4z^2)^{-3/2} + (r_{22}^2 + 4z^2)^{-3/2}]}{[r_{11}^{-1} - r_{12}^{-1} - r_{21}^{-1} + r_{22}^{-1}]}, \quad (1)$$

where r_{ij} is the distance between the current electrode C_i and the potential electrode P_j and z is the depth. Presented in Fig. 5 is the 1D interpretation of sensitivity for the floating electrode array used. The floating imaging array was designed to distribute the peak sensitivities for each dipole-dipole evenly along the logarithmic scale.

If there is variability in the electrical properties of the sediments in the *x* direction then 2D sensitivities are important (Loke 2004). If a distinct *x,z* location is considered and the contributions from $-\infty$ to ∞ in the *y* direction are added then the 2D sensitivity is defined by

$$F_{2D}(x,z) = \frac{1}{4\pi^2} \int_{-\infty}^{+\infty} \frac{x(x-a) + y^2 + z^2}{[x^2 + y^2 + z^2]^{1.5} [(x-a)^2 + y^2 + z^2]^{1.5}} dy, \quad (2)$$

where *x*, *y* and *z* define the point in space and *a* is the distance between the current electrode and the potential electrode. This is solved for each current and potential electrode pair and then all four permutations are combined to map the 2D sensitivity. Equation (2) was solved using Wolfram Research, Inc., Mathematica, Version 6.0 (2007) and the collated results are presented in Fig. 6. Three representative current (C) and potential (P) electrode configurations are presented: P_1P_2 separation $< C_1C_2$ separation, P_1P_2 separation = C_1C_2 separation and P_1P_2

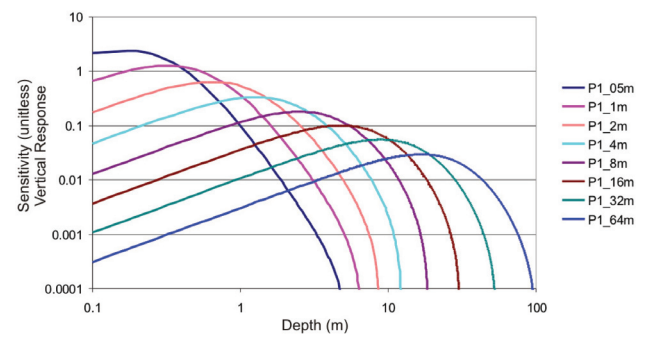


FIGURE 5 One dimensional sensitivity analysis of the floating electrical imaging array assuming a homogeneous half-space. The curves are labelled according to the potential electrode nearest the boat. The distance indicated for each P_1 electrode is the distance between the C_1 current electrode and the P_1 potential electrode.

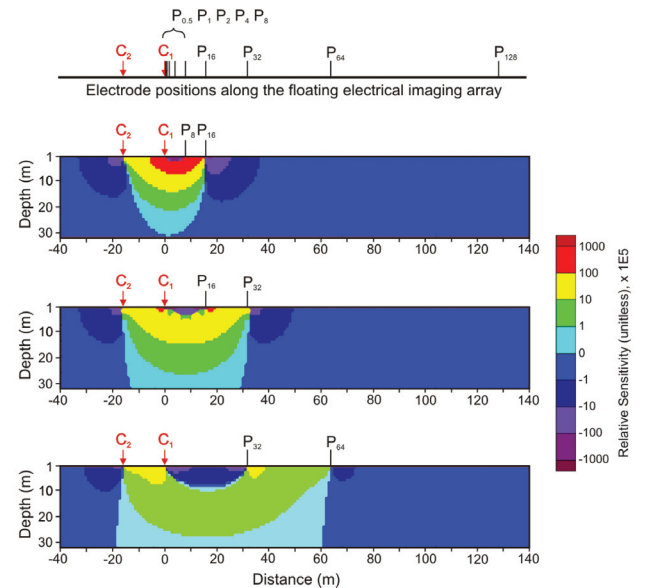


FIGURE 6 Two dimensional sensitivity analysis of the floating electrical imaging array. The two current electrodes are labelled C_1 and C_2 and the potential electrodes are labelled according to their distance from the C_1 electrode.

separation $> C_1C_2$ separation. Potential electrodes $P_{1,32m}$ and $P_{2,64m}$ have an effective depth close to the conductivity slice presented in the discussion below. For all quadrupoles the measurement is insensitive to the near-surface sediments between the current and the potential electrodes. For quadrupoles where the distance between P_1 and P_2 is less than the distance between C_1 and C_2 the array is highly sensitive to sediments within an arc from the C_1 electrode to the midpoint between P_1 and P_2 . When the electrodes in the quadrupole are evenly spaced the array is sensitive to sediments on an even arc from the midpoint between C_1C_2 to the midpoint between P_1P_2 . For cases where the distance between P_1P_2 is greater than the distance between C_1C_2 the array is sensitive to sediments beneath C_1C_2 and in the near-surface surrounding P_1 . For the electrode set $C_1C_2 P_{1,32m} P_{2,64m}$ at a depth of 25 m the positive sensitivity values are only 1% of the magnitude of those calculated for the upper 5 m of the half-space. In the analysis below the layered earth conductivity model at 16 m is compared to the sediments, groundwater quality and groundwater head change, which is above this level of low sensitivity.

DATA PROCESSING

Electrical imaging inversion

At each location the floating electrical conductivity sounding curve was inverted to generate a layered earth conductivity model. This model represents one estimate of the true electrical conductivity layering within the earth. The inversion algorithm used is a refinement of the 1D RINVERT inversion algorithm (Merrick and Poezd 1997; Allen and Merrick 2007). The forward modelling problem is solved using linear filter theory (O'Neill and Merrick 1984). The inverse modelling algorithm, which minimizes the difference between the forward modelled sounding curve and the field measured sounding curve, uses ridge regression in combination with the Marquardt algorithm. The automated starting model is derived from the apparent conductivity sounding curve, setting one layer centred on each quadrupole effective depth. The depth for the base of each layer is the

\log_{10} average of the effective depths of the corresponding quadrupole and the next largest quadrupole except for the last layer, which has no base. The depth of the layer nearest the bottom of the river is adjusted to the river bottom depth. Both the thickness and conductivity of this layer and all other layers are allowed to float during the inversion. In the numerical study of the automated inversion (Allen and Merrick 2007) it was determined that stable automatic inversions resulted if a vertical smoothness constraint (C_{vs}) as well as the extent of deviation from the starting layered model thicknesses (C_{dt}), were incorporated into the least squares measure of the goodness of fit between the forward modelled sounding curve and the field sounding curve. The additional constraints are defined by

$$C_{vs} = \frac{W_{vs} \sum_{i=2}^k \frac{2|\sigma_i - \sigma_{i-1}|}{k-1}}{k-1} \tag{3}$$

and

$$C_{dt} = W_{dt} \sqrt{\frac{\sum_{i=1}^{k-1} \sqrt{t_i - t_{o,i}}}{k-1}}, \tag{4}$$

where W_{vs} is a weight determined for the series of sounding curves (0.1 for this study), σ is the conductivity of the layer, k the number of layers, t the thickness of a layer, t_o is the original layer thickness and W_{dt} is a weight determined for the series of sounding curves (0.01 for this study). These constraints are then combined with the sum of squares (*SoS*) and sum of absolute deviations (*SoAD*) measured between the modelled and measured sounding curves via

$$\text{New Sum of Squares} = SoS + (W_{vs} + W_{dt}) (C_{vs} + C_{dt}) \tag{5}$$

and

$$\text{New Sum of Absolute Deviation} = SoAD + (W_{vs} + W_{dt}) (C_{vs} + C_{dt}) \tag{6}$$

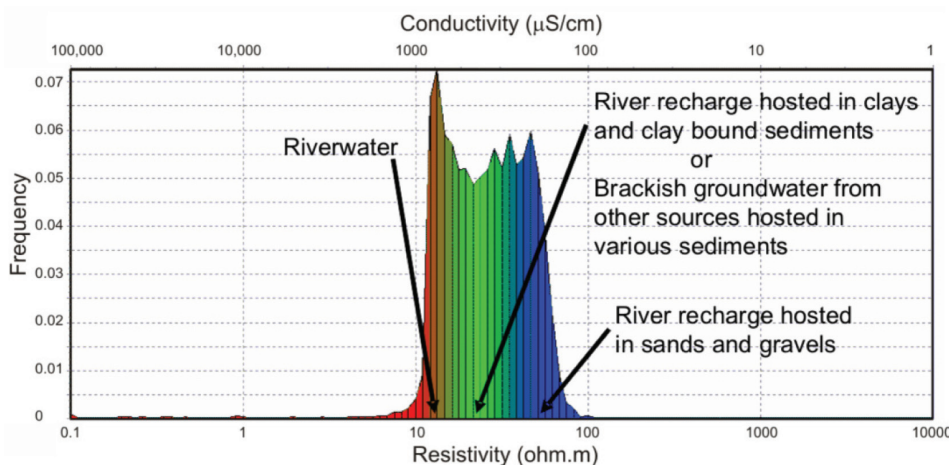


FIGURE 7 A histogram of the electrical conductivity imaging data collected beneath the lower Namoi River and the colour distribution used in Figs 8 and 9.

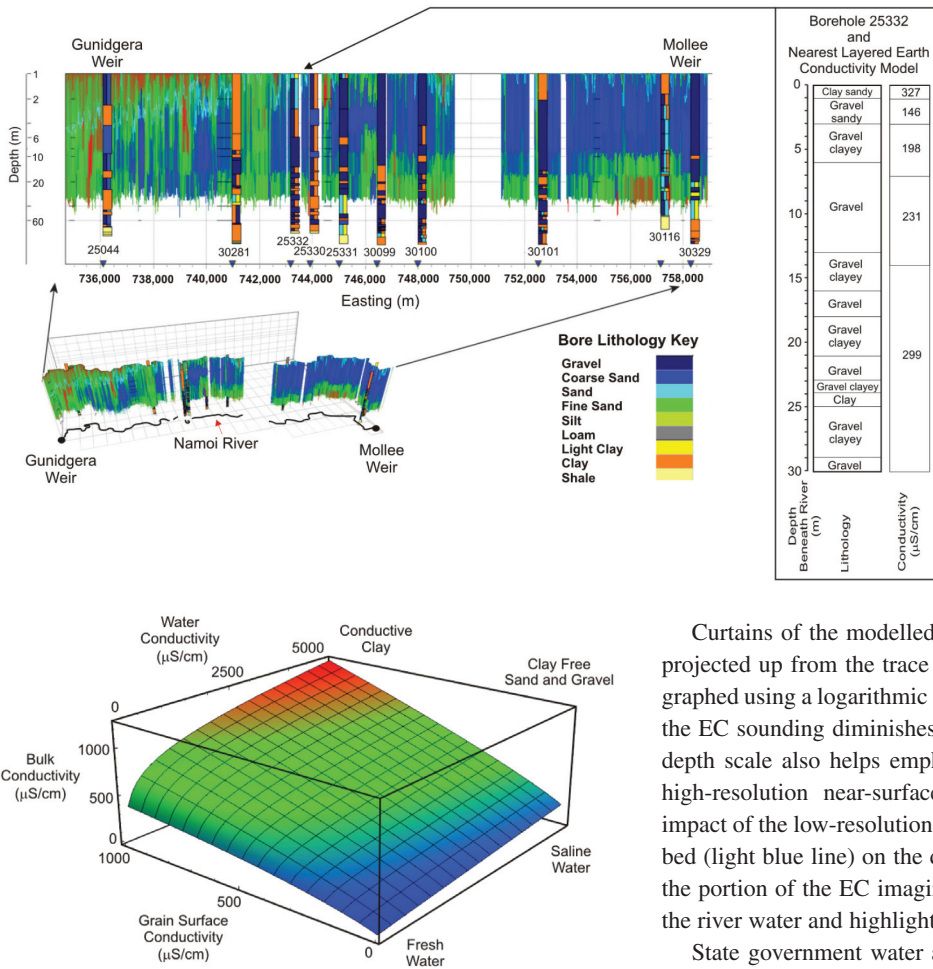


FIGURE 8 The electrical imaging layered earth conductivity model along the Namoi River. Borehole lithological logs are projected in front of the model. The lithological logs are presented with an 8 m depth shift upwards to offset the incision of the river into the alluvial plain. Electrical conductivity values are coloured using the scale presented in Fig. 7.

FIGURE 9 Bulk electrical conductivity as a function of pore water conductivity and grain surface conductivity calculated from the electrochemical effective medium model by Revil *et al.* (1998) fixing the cementation exponent to $m = 2$, the porosity to $(\phi) = 0.2$ and the cation Hittorf transport number to $t_{(+)} = 0.8$.

Comprehensive details of the inversion methodology are outlined in Allen and Merrick (2007).

Data collation and presentation

A histogram of all the electrical conductivity observations from the entire river segment surveyed is displayed in Fig. 7. The histogram was colour coded using an equal area colour scale. Due to a combination of the concentration of data acquired at shallow depths (sampling depths increase exponentially from about 0.1 m) and heating of near-surface water, which significantly raises EC, the river water peak in the histogram is skewed high. The high EC, near-surface water is not evident in any of the other figures as they have been clipped at 1 m because the upper river water is not the focus of this investigation. This colour coding of the electrical conductivity values is used in Figs 8 and 9.

Curtains of the modelled electrical conductivity values were projected up from the trace of the river (Fig. 8). The data were graphed using a logarithmic depth scale because the resolution of the EC sounding diminishes logarithmically with depth. Such a depth scale also helps emphasize the visual importance of the high-resolution near-surface data and diminishes the visual impact of the low-resolution data at depth. Projection of the river bed (light blue line) on the data allows interpreters to recognize the portion of the EC imaging cross-section that corresponds to the river water and highlights any boundary influences.

State government water authorities installed 588 monitoring boreholes in the region during the late 1950s through 1970s. The lithological logs from these boreholes near the river were plotted adjacent to the nearest section of the EC imaging cross-section (Fig. 8). The lithological logs have been shifted up 8 m relative to their collar referenced depths to account for the 8 m incision of the river within the otherwise flat floodplain. The unobservable top 8 m of all the logs is predominantly clay. Only lithological logs near the river have been plotted.

Interpreting the electrical conductivities of sediments

External information is required to determine if the observed change in the electrical conductivity of the sediments is due to varying pore water salinity, clay content, clay type, porosity or degree of saturation. The bulk conductivity of sediments depends non-linearly on the salinity of the groundwater. This non-linear relationship between the bulk conductivity of sediments, porosity, permeability and pore water salinity is well documented and has recently been reviewed by Friedman (2005), Niwas and de Lima (2003) and Shevvin *et al.* (2007). The non-linear relationship between pore water salinity and the bulk conductivity of the sediments has been measured in the laboratory for clays in nearby regions that have similar properties to the clays at the case study site (Emerson and Yang 1997). To calibrate this non-

linear relationship, detailed measurements of the bulk electrical properties of the sediments at various pore water salinities are needed. This level of calibration was not available for this project. For a quantitative investigation the electrical properties of the sediments in the region would need to be investigated in more detail.

The sensitivity of the bulk electrical conductivity (σ_b) of the sediment due to each of the major variables influencing the electrical conductivity is examined using the effective medium theory for porous media (Bussian 1983). The major variables are: pore water conductivity (σ_w), grain surface conductivity (σ_s), porosity (ϕ) and the cementation exponent (m), which depends on the aspect ratio of the grains and ranges from 1.5 for rounded quartz sand to 4 for clays (Kelly 1994). Revil *et al.* (1998) extended the effective medium theory to incorporate different charge carriers (anions and cations) and derived the following approximation

$$\sigma_b = \frac{\sigma_w}{F} \left[1 - t_{(+)}^f + F\xi + \frac{1}{2}(t_{(+)}^f - \xi) \left[\left(1 - \frac{\xi}{t_{(+)}^f}\right) + \sqrt{\left(1 - \frac{1}{t_{(+)}^f}\xi\right)^2 + \frac{4F}{t_{(+)}^f}\xi} \right] \right], \quad (7)$$

where $t_{(+)}^f$ is the fraction of electrical current carried in the free electrolyte by the cations,

$$\xi = \frac{\sigma_s}{\sigma_w} \quad (8)$$

and F is the formation factor defined by Archie (1942) as

$$\frac{1}{F} = \phi^m. \quad (9)$$

As the degree of saturation S_w decreases the conductivity of the sample decreases according to

$$\sigma_{ps} = \sigma_o S_w^n \quad (10)$$

where σ_{ps} is the conductivity of the partially saturated sediment and n is the saturation exponent.

The sensitivity of σ_b to σ_w and σ_s for saturated sediment is examined for σ_w ranging 100–5000 $\mu\text{S}/\text{cm}$, covering the values of groundwater EC measured in the boreholes and the σ_s range of 10–1000 $\mu\text{S}/\text{cm}$, covering values reported in the literature for clean sand and montmorillonite clays (Kelly 1994; Revil *et al.* 1998). The remaining variables were fixed to expected values for the sediments; setting $m = 2$, $\phi = 0.2$ and assuming Na^+ as the cation, $t_{(+)}^f = 0.38$. The results of the calculation are presented in Fig. 9. The non-linear relationship between σ_b and σ_w is clearly evident for high values of σ_s .

Comparing the calculated σ_b values in Fig. 9 to the histogram in Fig. 7, sediment EC values $> 1000 \mu\text{S}/\text{cm}$ consist of highly conductive clays (Ward *et al.* (1999) mapped extensive areas of smectite dominant soils in the region) with water EC near 5000 $\mu\text{S}/\text{cm}$. The middle of the histogram (green) represents highly electrically conductive clays with fresh pore water or

sediments containing a mixture of clay, sand and gravel with water EC of approximately 2500 $\mu\text{S}/\text{cm}$. The blue, low electrical conductivity end of the histogram represents sands and gravels wet with fresh water.

If highly unsaturated sediments, or low porosity consolidated and indurated rock were encountered the histogram in Fig. 7 would have been stretched to include much lower electrical conductivity values. Similarly, if saline groundwater was encountered, then this histogram would have been stretched to include much higher electrical conductivity values.

Regional borehole data

Some boreholes in the vicinity of the river have slotted intervals within the depth of investigation of the EC imaging (0–40 m). Groundwater EC data recorded by McLean (2003) from those boreholes were contoured using natural neighbour gridding (Watson 1992) to highlight any trends in the groundwater conductivity (Fig. 10). For comparison with the floating electrical imaging a slice taken at 16 m from the layered earth conductivity model in Fig. 8 has been superimposed on the map.

In Fig. 11 the difference between the pre-flood head from the peak head recorded after the flood has been contoured using natural neighbour gridding to create a map of groundwater head change resulting from the flood waters moving through the region. The rise in groundwater head near the river due to the flood waters occurs in similar locations near the river for each flooding event over the past 50 years. This flood recharge is shown for a single borehole located 200 m south of the river in Fig. 3. Superimposed on the groundwater flood recharge mound map is the 16 m depth slice from the layered earth conductivity model presented in Fig. 8.

DISCUSSION

In Fig. 8, it is clear that river water has a relatively high EC compared to the underlying sediment. The river water is the part of the projected image above the aqua coloured line in Fig. 8, which indicates the river bed depth. The state government water authority hydrograph data base indicated that the river water was 496–501 $\mu\text{S}/\text{cm}$ during the survey. In Fig. 7 it can be seen that the river water forms an orange coloured peak in the histogram. Below the aqua line in Fig. 8 the electrical conductivity is generally lower than the electrical conductivity of the river.

Based on the contouring of the borehole water EC data there appears to be little correlation between the borehole water EC readings and the river EC imaging (Fig. 10). In the south-east of the region near Mollee Weir some of the highest groundwater EC values have been recorded ($>500 \mu\text{S}/\text{cm}$), however much of the floating EC imaging data in this reach of the river displays low conductivity ($<450 \mu\text{S}/\text{cm}$). The reverse is displayed in the far west where low groundwater conductivity readings (450 $\mu\text{S}/\text{cm}$) occur where conductive sediment readings ($>500 \mu\text{S}/\text{cm}$) were recorded 16 m below the river. If water conductivity were dominating the measured bulk conductivity of the sediments then a

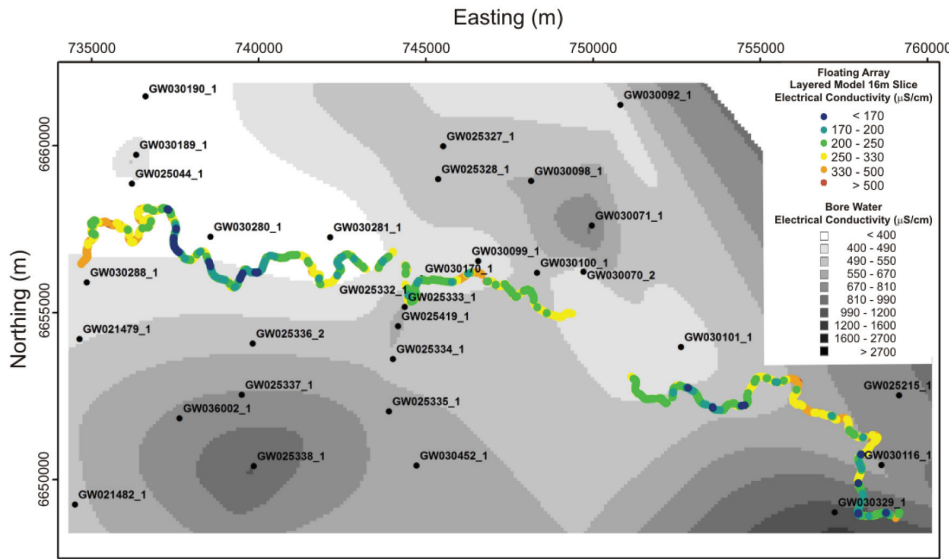


FIGURE 10 Narrabri Formation groundwater electrical conductivity (from McLean 2003) (gridded) using the natural neighbour algorithm. There are 31 sample points from the unconfined aquifer near the river. Superimposed on the map are the electrical conductivity values from a slice taken at 16 m beneath the river bed in the layered earth conductivity model presented in Fig. 8.

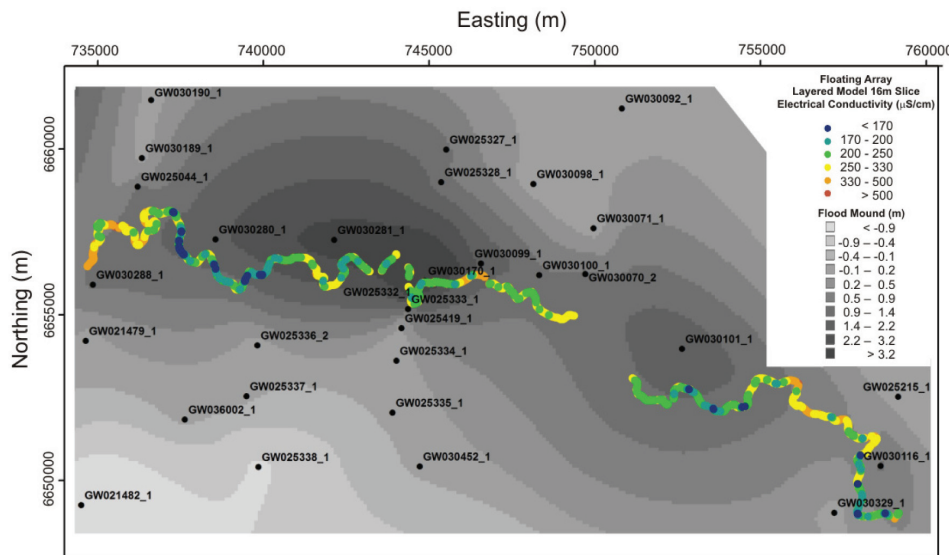


FIGURE 11 A map of the changes in borehole water levels resulting from the 1984 flood. There are 31 groundwater head measurements in the unconfined aquifer adjacent to the reach of the Namoi River surveyed. The data were gridded using the natural neighbour algorithm. Superimposed on the map are the electrical conductivity values from a slice taken at 16 m beneath the river bed in the layered earth conductivity model presented in Fig. 8.

strong positive correlation between water quality and bulk sediment conductivity would be expected. This is not apparent in the data. Part of this lack of correlation may be due to the low resolution of the borehole data.

The depth to the upper unconfined aquifer beneath the river varies from connected near Mollee weir, based on the water levels recorded at borehole location GW030116, to approximately 16 m in the west, based on water level readings taken at borehole locations GW025044 and GW030288. From equation (10) partially saturated sediments in the vadose zone should have a lower EC. This would suggest that the EC of the sediments beneath the river should decrease moving east to west in the upper portion of the layered earth conductivity model (Fig. 8). However, the reverse occurs with a general increase in sediment conductivity moving east to west. Thus, although the sediments beneath the river are not saturated the variability in the degree of saturation

is such that it does not strongly influence the measured EC of the sediments.

Clay type in the region does not vary substantially laterally but changes with depth. Sediments in the upper 10 m of the alluvial sequence are dominated by smectite, while kaolinite occurs in the sediments at depth. In the Quaternary sediments the clays are smectite rich with high cation exchange capacities of 200–500 mmol(+)/kg (Ward *et al.* 1999; Young *et al.* 2002). Where clay layers are present they should have a strong influence on the measured bulk conductivity, according to equation (7).

Figure 8 displays the EC imaging data along with graphical representations of the lithological logs near the river. Some of the lithological logs have been shifted to the nearest point along the EC imaging to help with the visual comparison of the conductivity data with the lithological logs. The Namoi River has meandered considerably during its history (Young *et al.* 2002) so this

can result in significant changes in sediment type within a few metres. Because none of the boreholes are right on the river, exact correlation between lithological logs and features in the EC imaging cross-section is not expected. The lithological logs are presented using colour codes that are, in places, compounded – for example, a clay bound gravel is presented by a teal (gravel) rectangle alongside an orange (clay) rectangle. The depth scale of the viewing space in Fig. 8 is logarithmic.

In the east of the EC imaging cross-section the upper 10 m is dominated by sediments with EC readings below 250 $\mu\text{S}/\text{cm}$. This corresponds to the predominant sand and gravel logs seen at borehole locations GW030329, GW030116, GW030101, GW030100 and GW030099. On the west of the cross-section sediment EC readings are above 300 $\mu\text{S}/\text{cm}$. This appears to correspond to the increased clay content recorded in the borehole logs located in the west, in particular the lithological log at borehole location GW030281 is mostly clay in the upper 20 m and this is adjacent to a near vertical relatively high conductivity band (green, >250 $\mu\text{S}/\text{cm}$) within the EC imaging cross-section.

Some of the EC changes in the EC imaging section are highlighted by looking at slices of the image in Fig. 8. At 2 m below the riverbed, EC increases moving east to west. The increase is attributed to increased clay content. Also evident from 2–6 m are sharp increases in EC at each southern meander bend between eastings 738,000 and 746,000. These rises in the EC of the sediments beneath the bends of the river are likely due to increased clay content in the underlying sediments, suggesting that the present river meander is migrating over historical overbank deposits. This hypothesis would need to be validated with detailed core logs at each of these bends in the river. However, the idea is supported by the work by Young *et al.* (2002) that indicated that historically the major channel of the Namoi River was further to the north in this region.

The continuity of the sand and gravel units is highlighted by the fact that above 8 m the eastern half of the EC imaging is dominated by low EC values (<250 $\mu\text{S}/\text{cm}$, blue). These sediments provide a permeable hydraulic link between the river and the underlying aquifers. At 16 m on the eastern half of the layered earth conductivity model is the section dominated by higher EC sediments (>250 $\mu\text{S}/\text{cm}$, green and red). This would mean that there is likely to be reduced vertical movement of groundwater to lower depths. Small intervals of several hundred metres in length of low EC sediments (blue intervals) are seen in the interval 16 m and 32 m. The horizontal intervals of sand and gravel in this depth range are possibly permeable pathways that allow recharge to the underlying aquifers.

In Fig. 11 the change in head recorded in the boreholes due to the 1984 flood were contoured. The groundwater head mound extends mostly to the north, supporting the interpretation that sand and gravel palaeochannels extend to the north. There is a trough in the groundwater head mound at borehole location GW025044 and just south of this borehole it is inferred from the EC imaging that

this interval is dominated by clayey sediments. These clay units appear to have an impact on the local groundwater head. Conductive sediments also occur in the trough between GW030099 and GW030070 and the trough north-west of GW030116.

CONCLUSIONS

Dedicated boreholes for examining the hydraulic connection between the Namoi River and the underlying aquifer are required to further validate the findings presented in this paper. However, using nearby government groundwater monitoring boreholes it is apparent that in this region the EC of the sediments is strongly influenced by the clay content and to a lesser extent the salinity of the pore water.

For sediments beneath the river there does not seem to be any appreciable change in the measured sediment EC relating to the measured groundwater head, thus sediments above the water table still have a high degree of saturation. In the western half of the river EC imaging, where the water table is known to exist 10–20 m below the river bed, prior to this investigation it would have been reasonable to expect that sediments above the water table would have a lower degree of saturation and therefore a lower EC reading. This did not appear to be the case.

EC imaging mapped mostly sands and gravels from easting 758,000 through to easting 742,000 in the upper 10 m of the sediments beneath the river. Recharge most likely occurs along this entire stretch. At approximately 16 m below the river the EC of the sediments increases significantly, suggesting the presence of substantial clay. These clayey units would form an aquitard and hinder recharge to the underlying Gunnedah Formation.

The 1984 flood is observable in the piezometers located in the underlying Gunnedah Formation (Fig. 3), so there is clear evidence that flood waters do migrate to depth. Beneath the Namoi River there appears to be a recharge pathway to the Gunnedah Formation in the interval between eastings 737,000 and 740,000, with a much smaller sand and gravel zone at easting 753,500.

At this case study location floating EC imaging provided much higher resolution sediment EC data than had been collected to date. These sediment EC data did not appear to map water quality changes or changes relating to the field capacity of the sediments. When visually compared to lithological logs recorded in boreholes adjacent to the river, the EC imaging correlated with the major changes in sediment type observed in the boreholes. Without the borehole control it would not have been possible to interpret the floating EC imaging but with borehole control the EC imaging provided valuable information that ties the data from the boreholes together and fills the section between them. The floating EC imaging also provides information directly beneath the river where no core log details are available. The EC imaging indicates a likely recharge pathway to the Gunnedah Formation exists near easting 739,000, northing 6,666,500.

It is shown that there is a tendency for sediments with low electrical conductivity to occur above intervals where groundwater mounds occur after flood waters migrate along the river. This

can be attributed to the higher sediment EC readings corresponding to higher clay content. The higher clay content in the sediment would impede vertical recharge to the unconfined aquifer at these locations. The aquifer recharging waters appear to migrate via the sands and gravels pooling at the water table before slowly dissipating.

ACKNOWLEDGEMENTS

The financial contributions from the Cotton Catchment Communities CRC, Cotton Research Development Corporation, Namoi Catchment Management Authority, University of Technology, Sydney (UTS) and the University of New South Wales (UNSW) are acknowledged. We would also like to thank Associate Professor Noel Merrick, Lorraine Dixon (UTS) and Professor Ian Acworth (UNSW) for managing the administration of the project. We appreciate the help of Dr B. Giambastiani for her ArcGIS processing of the 2D maps and we thank the reviewers for their careful reading of the manuscript and their suggestions.

REFERENCES

- Allen D.A. 2007. *Electrical conductivity imaging of aquifers connected to watercourses: A thesis focused on the Murray Darling Basin, Australia*. PhD thesis, University of Technology, Sydney, Australia.
- Allen D.A. 2007b. *HydroGeoImager Version 1.1 software*. Available from <http://www.groundwaterimaging.com> (access verified 20th January 2009).
- Allen D. and Merrick N. 2007. Robust 1D inversion of large towed geoelectric array datasets used for hydrogeological studies. *Exploration Geophysics* **38**, 50–59.
- Archie G.E. 1942. The electrical resistivity log as an aid in determining some reservoir characteristics. *Transactions of the American Institute of Mining and Metallurgical and Petroleum Engineers* **146**, 54–62.
- Ball L.B., Kress W.H., Steele G.V., Cannia J.C. and Anderson M.J. 2006. Determination of canal leakage potential using continuous resistivity profiling techniques, Interstate and Tri-State Canals, Western Nebraska and Eastern Wyoming, 2004. US Department of the Interior, US Geological Survey, Scientific Investigations report 2006-5032.
- Barrett B., Heinson G., Hatch M. and Telfer A. 2002. Geophysical methods in saline groundwater studies: Locating perched water tables and fresh-water lenses. *Exploration Geophysics* **33**, 115–121.
- Barrett B., Heinson G., Hatch M. and Telfer A. 2006. River sediment salt-load detection using a water-borne transient electromagnetic system. *Journal of Applied Geophysics* **58**, 29–44.
- Bussian A.E. 1983. Electrical conductance in porous medium. *Geophysics* **48**, 1258–1268.
- Calf G.E. 1978. An investigation of recharge to the Namoi Valley aquifers using environmental isotopes. *Australian Journal of Soil Research* **16**, 197–207.
- Cherkauer D.S. and Taylor R.W. 1990. The spatially continuous determination of groundwater flow to surface water bodies: Application to the connecting channels between lakes Huron and Erie. *Journal of Hydrology* **114**, 349–369.
- Cherkauer D.S., Taylor R.W. and Bradbury K.R. 1987. Relation of lake bed leakance to geoelectrical properties. *Ground Water* **25**, 135–140.
- Davis J.C. 2002. *Statistics and Data Analysis in Geology*, 3rd edn. Wiley and Sons.
- Day-Lewis F.D., White E.A., Johnson C.D., Lane J.W. and Belaval M. 2006. Continuous resistivity profiling to delineate submarine groundwater discharge – Examples and limitation. *The Leading Edge* **25**, 724–728.
- Edwards L.S. 1977. A modified pseudosection for resistivity and IP. *Geophysics* **42**, 1020–1036.
- Emerson D.W. and Yang Y.P. 1997. Effects of water salinity and saturation on the electrical resistivity of clays. *Preview* **68**, 19–24.
- Friedman S.P. 2005. Soil properties influencing apparent electrical conductivity: A review. *Computers and Electronics in Agriculture* **46**, 45–70.
- Hatch M., Fitzpatrick A., Munday T., Heinson G., 2007. An assessment of “in-stream” survey techniques along the Murray River, Australia. ASEG 2007 meeting, Perth, Western Australia, Expanded Abstracts.
- Kelly B.F.J. 1994. *Electrical properties of sediments and the geophysical detection of ground water contamination*. PhD thesis. The University of New South Wales, Australia.
- Loke M.H. 2004. Tutorial: 2-D and 3-D electrical imaging surveys. Available from <http://www.geoelectrical.com>.
- Loke M.H. and Lane J.W. 2004. Inversion of data from electrical resistivity imaging surveys in water-covered areas. *Exploration Geophysics* **35**, 266–271.
- Mansoor N. and Slater L. 2007. Aquatic electrical resistivity imaging of shallow-water wetlands. *Geophysics* **72**, F211–F221.
- Martin H.A. 1979. Stratigraphic palynology of the Mooki Valley, New South Wales. *Journal and Proceedings of the Royal Society of New South Wales* **112**, 71–78.
- Martin H.A. 1981. Stratigraphic palynology from shallow bores in the Namoi River and Gwydir River valleys, north-central New South Wales. *Journal and Proceedings of the Royal Society of New South Wales* **113**, 81–87.
- Martin H.A. 1991. Tertiary stratigraphic palynology and palaeoclimate of the inland systems in New South Wales. In: *The Cainozoic in Australia: A Re-appraisal of the Evidence*, Vol. 18 (ed. M.A.J. Williams, P. de Deckker and A.P. Kershaw), pp.181–194. Geological Society of Australia.
- McGillivray P.R. and Oldenburg D.W. 1990. Methods for calculating Fréchet derivatives and sensitivities for the non-linear inverse problem: A comparative study. *Geophysical Prospecting* **38**, 499–524.
- McLean W.A. 2003. *Hydrogeochemical evolution and variability in a stressed alluvial aquifer system: Lower Namoi River catchment, NSW*. PhD thesis, University of New South Wales, Sydney, Australia.
- Merrick N.P. 1997. A new resolution index for resistivity electrode arrays. *Exploration Geophysics* **28**, 106–109.
- Merrick N.P. 2000. *Optimisation techniques for groundwater management*. PhD thesis, University of Technology, Sydney, Australia.
- Merrick N.P. and Poezd E. 1997. RINVERT for Windows software for the interpretation of resistivity soundings. *Exploration Geophysics* **28**, 110–113.
- Niwas S. and de Lima O.A.L. 2003. Aquifer parameter estimation from surface resistivity data. *Ground Water* **41**, 94–99.
- NSWG 2007. Historic data CD PINNEENA for groundwater works. New South Wales Government.
- Nyquist J.E., Freyer P.A. and Toran L. 2008. Stream bottom resistivity tomography to map ground water discharge. *Ground Water* **46**, 561–569.
- O’Neill D.J. and Merrick N.P. 1984. A digital linear filter for resistivity sounding with a generalized electrode array. *Geophysical Prospecting* **32**, 105–123.
- Rahman M. 2005. *A statistical analysis of hydrograph data for estimating recharge in the lower Namoi Valley, NSW, Australia*. MSc thesis, University of Technology, Sydney, Australia.
- Revil A., Cathles L.M., Losh S. and Nunn J.A. 1998. Electrical conductivity in shaly sands with geophysical applications. *Journal of Geophysical Research* **103**, 23925–23936.
- Roy A. and Apparao A. 1971. Depth of investigation in direct current methods. *Geophysics* **36**, 943–959.

- Shevnnin V., Mousatov A., Ryjov A. and Delgado-Rodriquez O. 2007. Estimation of clay content in soil based on resistivity modelling and laboratory measurements. *Geophysical Prospecting* **55**, 265–275.
- Snyder D.D., MacInnes S.C., Raymond M.J. and Zonge K.I. 2002. Continuous resistivity profiling in shallow marine and fresh water environments. Proceedings – Symposium on the Application of Geophysics to Engineering and Environmental Problems (SAGEEP), Las Vegas, Nevada, USA, Expanded Abstracts, 13GSL4.
- Tan K.P., Berens V., Hatch M. and Lawrie K. 2007. Determining the suitability of in-stream NanoTEM for delineating zones of salt accession to the River Murray: A review of survey results from Loxton, South Australia, CRC LEME open file report 192.
- Triantafilis J., Odeh I.O.A., Minasny B. and McBratney A.B. 2003. Elucidation of physiographic and hydrogeological units using fuzzy k-means classification of EM34 data in the lower Namoi valley. *Environmental Modelling and Software* **18**, 667–680.
- Ward W.T. 1999. Soils and landscapes near Narrabri and Edgeroi, NSW, with data analysis using fuzzy k-means. CSIRO Technical Report 22/99.
- Ward W.T., McTainsh G., McGarry D. and Smith K.J. 1999. The soils of the agricultural research station at 'Myall Vale', near Narrabri, NSW, with data analysis by fuzzy k-means. CSIRO Technical Report 21/99.
- Watson D.F. 1992. *Contouring: A Guide to the Analysis and Display of Spatial Data*. Pergamon.
- Williams R.M., Merrick, N.P. and Ross J.B. 1989. Natural and induced recharge in the lower Namoi valley, New South Wales. In: *Groundwater Recharge, Proceedings of the Symposium on Groundwater Recharge, Mandurah* (ed. M.L. Sharma), pp. 239–253. A.A.Balkema, Rotterdam.
- Wolfram Research Inc. 2007. *Mathematical Edition: Version 6.0*. Wolfram Research, Inc., Champaign, Illinois.
- Young R.W., Young A.R.M., Price D.M. and Wray R.A.L. 2002. Geomorphology of the Namoi alluvial plain, northwestern New South Wales. *Australian Journal of Earth Sciences* **49**, 509–523.





MALÅ GPR, simply the best of GPR solutions!

With the best available technology and built by Swedish quality products, offer the user-friendly MALÅ GPR Systems effective and flexible GPR solutions.

Find out today what MALÅ GPR can do for you!

Contact us now for further information www.malags.com



Corporate Headquarters
MALÅ Geoscience AB
Skolgatan 11, SE-930 70
Malmö Sweden
Phone: +46 953 345 50,
Fax: +46 953 345 67
E-mail: sales@malags.com

Offices
USA: MALÅ Geoscience USA, Inc., 2040 Savage Rd. Box 80430, Charleston, SC 29416
Phone: +1 843 852 5021, Fax: +1 843 769 7392, E-mail: sales.usa@malags.com
China: MALÅ Geoscience (China), Room 2604, Yuan Chen Xin BLDG, No.12 Yu Min Road Chao Yang District, Beijing 100029
Phone: +86 108 225 0728, Fax: +86 108 225 0813, E-mail: sales@malags.com



www.malags.com



Geomatrix

EARTH SCIENCE LTD

Your Geophysical Source!
Sales, rental and service

Our expertise covers mineral exploration, all types of near surface surveys, marine geophysics, UXO and surveys for other manmade hazards

T: +44 (0)1525 383438
E: sales@geomatrix.co.uk
www.geomatrix.co.uk

20 Eden Way, Pages Industrial Park, Leighton Buzzard, Beds LU7 4TZ. UK.